ITD Formulation for the Currents on a Plane Angular Sector

Stefano Maci, *Member, IEEE*, Matteo Albani, *Member, IEEE*, and Filippo Capolino, *Member, IEEE*

Abstract— **Approximate high-frequency expressions for the currents induced on a perfectly conducting plane angular sector are derived on the basis of the incremental theory of diffraction (ITD). These currents are represented in terms of those predicted by physical optics (PO) plus fringe contributions excited by singly and doubly diffracted (DD) rays at the two edges of the angular sector. For each of these two contributions, additional currents associated to vertex diffracted rays are introduced that provide continuity at the relevant shadow boundary lines. The transition region of DD rays is described by a transition function involving cylinder parabolic functions. The asymptotic solution presented here is constructed in such a way to satisfy far from the vertex the expected edge singularities, which tend to be the same as those predicted by the exact solution of the half plane. Numerical results are compared with the exact solution of the same problem and with moments method results for scattering from polygonal plates.**

Index Terms—**Geometrical theory of diffraction, high-frequency techniques, incremental theory of diffraction, physical optics.**

I. INTRODUCTION

A perfectly conducting corner at the interconnection of two straight edges, joined by a plane angular sector is a basic canonical problem for the high-frequency description of electromagnetic scattering phenomena. This problem can be used within the framework of the geometrical theory of diffraction (GTD) [1] and of its uniform extension (uniform theory of diffraction (UTD) [2]), to find diffraction coefficients for application to complex structures. The same canonical problem is also useful to obtain an estimate of fringe currents close to vertex discontinuity. Referring to terminology of the physical theory of diffraction (PTD) [3], [4], fringe currents denote those currents that are induced on the metallic faces of the plane angular sector by the diffracted fields; their radiation in free-space provides high-frequency augmentation of the physical optics (PO) field. Simple tools for providing an estimate of the currents associated to vertex discontinuity is useful for improving without substantial additional efforts, those numerical codes that use the direct integration of the PO currents to predict radar cross section (RCS) or antenna radiation. This is the major motivation in developing asymptotic current expressions for the basic canonical problems of a plane angular sector illuminated by a plane wave.

The approximate solution presented here exhibits useful properties. First, it includes contributions from first- and second-order UTD grazing rays, including slope effects far from their pertinent shadow boundaries; next, it provides via simple transition functions a uniform distribution of the currents everywhere; finally, it exhibits away from the vertex the appropriate behavior near the edges, which is embedded in the exact solution for the local half-planes.

The problem of the plane angular sector has been extensively treated in the literature by resorting to both exact and approximate high-frequency solution. The exact solution of the scalar problem for soft boundary conditions and 90° plane angular sector was obtained by Radlow [5], who used the Wiener–Hopf technique; his work was recently extended to the electromagnetic case by Albertsen [6]. For arbitrary corner angle, the exact electromagnetic solution was first found by Satterwhite and Kouyoumjian [7], [8]; however, the series expansion representation of the solution is slowly convergent when the distance from the tip increases and no practical asymptotic approximation has been found yet. An alternative derivation of the same solution was given in [9]; in the works by Smyshlyaev [10], [11] the exact solution was obtained as a particular case of an elliptical degenerated cone. The solution in [7], [8] was used in [12] to obtain an interpolation of the fringe currents in a region close to the tip after extracting the UTD dominant terms. In [13], a hybrid method of moments (MoM)-UTD procedure was applied to a square plate in order to derive approximate analytical expressions for the currents on a right-angled plane angular sector.

Asymptotic fringe currents have also been derived by using approximate, but practical high-frequency solutions, which are based on modeling the vertex geometry as a superposition of two or more wedges. In this framework, first-order vertex diffraction coefficients were formulated in [14] in order to compensate for the discontinuity of first-order UTD diffraction contributions without including second-order interactions between the edges. Double diffraction at skew edges has been treated in [15], [16] neglecting the contribution of the vertex. The formulation presented in [16], which is based on the extension of the spectral formulation given in [17] for parallel edges, also includes double interactions for soft polarization. In [18] and [19], the scattering from polygonal structures was treated within the framework of PTD including second order interactions; in [18] vertex contributions were also included.

Recently, vertex diffraction coefficients have been derived in the plane-wave far-field regime by the application of the induction theorem [20]. These coefficients account for second-

order interactions between the two edges and explicitly satisfy reciprocity. The same formulation has been used in [21] to find, via spectral synthesis, a uniform solution for observation points at finite distances from the tip. The solution in [21] as well as other solutions presented in the literature [14], [18] are expressed in terms of a generalized Fresnel integral [22], which may appear to require significant computional efforts when the currents are used in a radiation integral. Nevertheless, the generalized Fresnel integral is essentially required to describe the field at those observation points where transition regions of different nature overlap; when the observation point is on the surface (i.e., when calculating the currents) such situations never occur, so that the currents may be conveniently described by ordinary Fresnel integrals. This also provides more manageable expressions for users familiar with UTD.

It should also be noted that in applying the above-mentioned approximate solutions to calculate the field on the plane angular sector itself, practical inconveniences may occur. Indeed, the high-frequency vertex coefficients typically are not valid close to and at the two edges while it should be desirable to construct currents that exhibit there the appropriate behavior. The accurate description of the near-edge behavior becomes particularly important when the electric currents are used to find couplings with magnetic distributions located on the surface, as it occurs when dealing with radiation of apertures on finite ground planes.

For the reasons described above (i.e., to avoid the use of generalized Fresnel functions in radiation or coupling integrals and to preserve the near-edge behavior), in this paper, the expressions of the fringe currents are derived by a completely different formulation with respect to our previous solutions [16], [20], [21]. The problem is formulated by distributing, on the semi-infinite edges of the plane angular sector, first- and second-order incremental diffraction coefficients based on the incremental theory of diffraction (ITD) [23], [24]. The use of ITD in this application is particularly effective, since the relevant incremental diffraction contributions satisfy the boundary conditions (BC's) of their pertinent tangent canonical wedge, so that they are expected to provide an accurate estimate of the currents. A significant example is shown in [25], where a circular perfectly conducting disc illuminated by a vertical dipole was treated.

In deriving the present solution, terms of order up to $(kr)^{-2}$ (where r is the distance from the tip) are retained in the asymptotic expansion, unlike our previous work [21], in which only order up to $(kr)^{-1}$ was considered. These higher order contributions are consistent with those required to reconstruct the near-edge behavior, that are of order $(kr)^{-2}$ owing to their reactive nature.

In the present formulation, the ITD fringe currents are decomposed into the sum of two contributions that are associated with single and double diffraction mechanisms, respectively. Both these contributions are, in turn, decomposed into two terms that are associated with the edges and the vertex, respectively. In Section II, the field representation is presented; the currents relevant to single and double diffraction mechanisms are formulated in Sections III and IV, respectively. Their
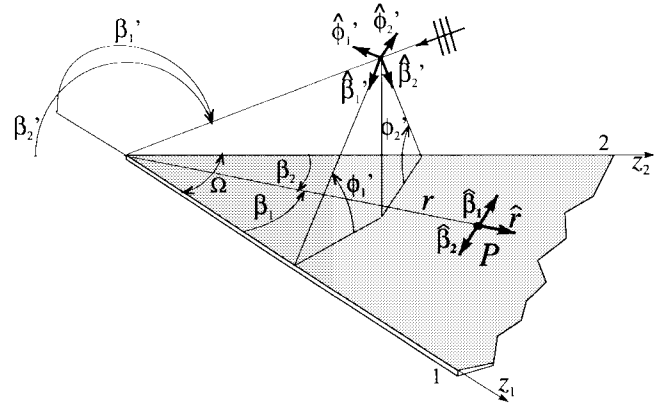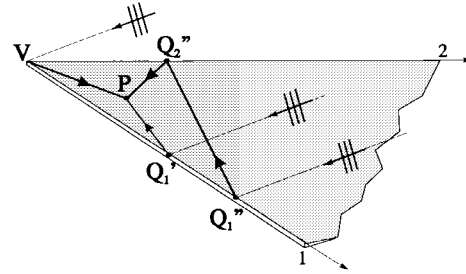

Fig. 1. Geometry of the plane anular sector.

Fig. 2. Ray contributions associated to edge 1 of the plane angular sector; a singly diffracted ray originates at Q'_1; a vertex ray arises from the vertex V; a DD ray arises from a point Q''_2 on edge 2 after diffracting at the point Q''_1 on edge 1.

behavior is discussed to find the convenient terms to retain in the asymptotic expansion. Finally, in Section V, this estimate of the currents is compared with that calculated from the exact solution [7], [8]. Also, examples of radar cross section of polygonal plates are presented and compared with MoM calculations.

II. FIELD REPRESENTATION

The geometry at a plane angular sector with aperture angle Ω is shown in Fig. 1. At both edges 1 and 2, a spherical coordinate system (r, β_n, ϕ_n) with relevant unit vectors $(\hat{r}, \hat{\beta}_n, \hat{\phi}_n)$ is introduced, with its origin at the tip. A plane wave illumination is assumed with direction of incidence (β'_n, ϕ'_n). The incident magnetic field $\vec{H}^i$ at the vertex is defined by its components $H^i_{\beta_n}$ and $H^i_{\phi_n}$, along the unit vectors $\hat{\beta}'_n$, and $\hat{\phi}'_n$, respectively. In our description, the total current $\vec{J}$ is represented as

$$\vec{J} = \vec{J}^{PO} + \vec{J}^f_1 + \vec{J}^f_2 \tag{1}$$

where $\vec{J}^{PO} = 2\hat{n} \times \vec{H}^i$ ($\hat{n}$ normal to the face) denotes the PO current and $\vec{J}^f_1$, $\vec{J}^f_2$, are fringe current contributions induced by the diffracted field arising from edge 1 and 2, respectively. The ray contributions arising from edge 1 are those represented in Fig. 2. In particular: 1) a singly diffracted ray originates at Q'_1; 2) a vertex ray arises from the tip; and 3) a doubly diffracted (DD) ray arises from a point Q''_2 on edge 2 after diffracting at the point Q''_1 on edge 1. Analogous mechanisms occur at edge 2. In the following, we will discuss only the
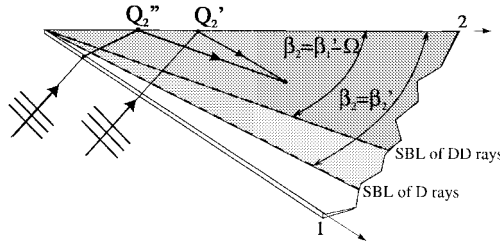
Fig. 3. Shadow boundary lines (SBL's) of the currents induced by singly ($\beta_2 = \beta_2'$) and doubly ($\beta_2 = \beta_1' - \Omega$) diffracted rays.

contributions $\vec{J}_1^f$ associated to the rays depicted in Fig. 1(b), namely those in which the first diffraction occurs at edge 1; the other contribution $\vec{J}_2^f$ can be easily obtained from $\vec{J}_1^f$ by interchanging 1 by 2 and introducing a minus sign (due to the left-handness of the reference system assumed for edge 2).

Let us denote by $\vec{J}_1^d$ and $\vec{J}_1^{dd}$ the currents induced by the singly and DD rays, respectively. In a ray-optics representation, these contributions are discontinuous when the observation point is such that Q_n' or Q_n'' ($n = 1, 2$) disappear from the vertex, respectively, as depicted in Fig. 3. This occurs at the shadow boundary lines (SBL's) defined by $\beta_1 = \beta_1'$ and $\beta_2 = \beta_1' - \Omega$, respectively. The discontinuities $\vec{J}_1^d$ and $\vec{J}_1^{dd}$ have to be compensated by current contributions associated to vertex diffracted rays. The latter are conveniently subdivided into two terms $\vec{J}_1^v$ and $\vec{J}_1^{vv}$, that are intended to provide the continuity of $\vec{J}_1^d$ and $\vec{J}_1^{dd}$, respectively. The terms $\vec{J}_1^v$ and $\vec{J}_1^{vv}$ will be referred to as currents induced by vertex rays of the first and second kind, respectively. Thus, our representation of the fringe current $\vec{J}_1^f$ is

$$\vec{J}_1^f = \vec{J}_1^{f'} + \vec{J}_1^{f''} \tag{2}$$

where

$$\vec{J}_1^{f'} = \vec{J}_1^d + \vec{J}_1^v \tag{3}$$

and

$$\vec{J}_1^{f''} = \vec{J}_1^{dd} + \vec{J}_1^{vv}. \tag{4}$$

In Sections III and IV, high-frequency approximations of the two contributions $\vec{J}_1^{f'}$ and $\vec{J}_1^{f''}$ are derived, respectively.

III. CURRENT INDUCED BY SINGLY DIFFRACTED RAYS AND BY VERTEX RAYS OF THE FIRST KIND

Let us consider an infinite half-plane with its edge aligned with edge 1 of the plane angular sector. The current contributions relevant to $H_{\beta_1}^i$ and $H_{\phi_1}^i$ are denoted by superscripts H and E, respectively. These contributions correspond to hard and soft boundary conditions on the faces of the angular sector, respectively. We denote by $\vec{J}_{1\infty}^d(\beta_1')$ the summation of the fringe currents on the two faces of this infinite structure; these are expressed in exact closed form as [26]

$$\vec{J}_{1\infty}^d(\beta_1') = \vec{J}_{1\infty}^{dE}(\beta_1') + \vec{J}_{1\infty}^{dH}(\beta_1') \tag{5}$$

where

$$\vec{J}_{1\infty}^{dH}(\beta_1') = -2H_{\beta_1'}^i \frac{e^{-jkr \cos(\beta_1 - \beta_1')}}{\sqrt{2j\pi kr \sin \beta_1' \sin \beta_1} \cos\left(\dfrac{\phi_1'}{2}\right)}$$
$$\times \left[F(kr\delta_1')\hat{s}_1(\beta_1') + \frac{F_s(kr\delta_1') \cos \beta_1'}{2jkr \sin \beta_1' \sin \beta_1} \hat{z}_1 \right] \tag{6}$$

and

$$\vec{J}_{1\infty}^{dE}(\beta_1') = 2H_{\phi_1'}^i \frac{e^{-jkr \cos(\beta_1 - \beta_1')}}{\sqrt{2j\pi kr \sin \beta_1' \sin \beta_1}}$$
$$\times \frac{\sin\left(\dfrac{\phi_1'}{2}\right)}{\cos^2\left(\dfrac{\phi_1'}{2}\right)} \left[\frac{F_s(kr\delta_1')}{2jkr \sin \beta_1' \sin \beta_1} \hat{z}_1 \right] \tag{7}$$

in which

$$\delta_1' = 2 \sin \beta_1 \sin \beta_1' \cos^2\left(\frac{\phi_1'}{2}\right). \tag{8}$$

In (6), (7)

$$\hat{s}_1(\beta_1') = \sin(\beta_1' - \beta_1)\hat{\beta}_1 + \cos(\beta_1' - \beta_1)\hat{r} \tag{9}$$

is the unit vector directed along the grazing ray and $\hat{z}_1$ is the unit vector along edge 1. Furthermore

$$F(y) = 2j\sqrt{y}e^{jy} \int_{\sqrt{y}}^{\infty} e^{-jt^2} \, dt;$$
$$-\frac{3\pi}{2} < \arg(y) \le \frac{\pi}{2} \tag{10}$$

and

$$F_s(y) = 2jy(1 - F(y)) \tag{11}$$

are the UTD transition function and the UTD slope-transition function, respectively.

The current contributions along $\hat{z}_1$ in (6) and (7) become dominant approaching the edges, where they exhibit singularities. It is worth noting that (6) and (7) do not derive from any kind of asymptotic approximation of the half-plane solution, but they are exact; consequently, they satisfy the edge conditions and provide the exact reactive field components close to the edge.

According to the ITD localization process, the current of the canonical problem is represented as

$$\vec{J}_{1\infty}^d(\beta_1') = \int_{-\infty}^{\infty} \vec{I}_1^d(z_1')e^{-jkz_1' \cos \beta_1'} \, dz_1'. \tag{12}$$

The above expression can be thought of as a superposition of an infinite distribution of incremental diffraction contributions $\vec{I}_1^d(z_1')$ that are localized along edge 1 and excited with a phase factor $\exp(-jkz' \cos \beta')$ which is dictated by the incident plane wave.
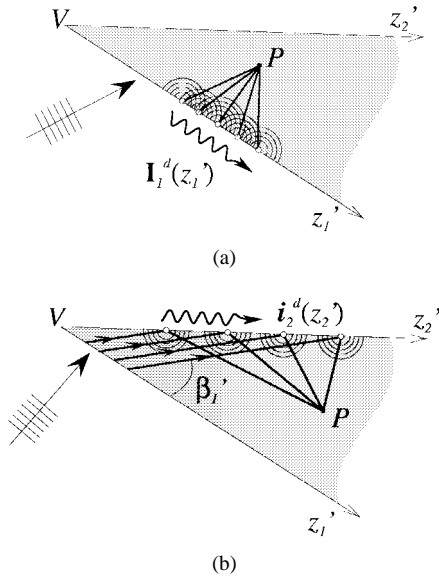
Fig. 4. ITD synthesis of the diffraction mechanisms. (a) Singly diffracted incremental contributions from edge 1. (b) DD incremental contribution at edge 2.

The above expression establishes a Fourier transform pair relationship between the incremental current contribution $\vec{I}_1^d$ and the current $\vec{J}_{1\infty}^d$ of the canonical half plane. Thus, $\vec{I}_1^d$ can be calculated as inverse Fourier transformation of $\vec{J}_{1\infty}^d$, i.e.,

$$\vec{I}_1^d(z_1') = \frac{k}{2\pi} \int_{C_{\theta_1}} \vec{J}_{1\infty}^d(\theta') \sin\theta_1 e^{jkz_1' \cos\theta_1} d\theta_1 \qquad (13)$$

in which C_{θ_1} is the contour $(-j\infty, \pi + j\infty)$. The contribution $\vec{I}_1^d(z_1')$ represents an incremental fringe current outgoing from the point z_1' on edge 1, with a spherical spreading factor. As depicted in Fig. 4(a), the fringe current contribution $\vec{J}_1^{f'}$ relevant to the semi-infinite edge can be constructed by superimposing the spherical incremental fringe currents on the semi-infinite extent $z_1' \geq 0$ of the edge, namely

$$\vec{J}_1^{f'} = \int_0^\infty \vec{I}_1^d(z_1') e^{-jkz_1' \cos\beta_1'} dz_1'. \qquad (14)$$

This integral provides two asymptotic contributions for large kr. The first one ($\vec{J}_1^{dH} + \vec{J}_1^{dE}$) arises from the stationary phase point of the integrand occurring at Q_1'; and it may be easily recognized as the one produced by the singly diffracted ray. The second contribution ($\vec{J}_1^{vH} + \vec{J}_1^{vE}$) arises from the endpoint at the vertex, and provides the desired continuity of the currents $\vec{J}_1^{f'}$ at the single diffraction SBL ($\beta_1 = \beta_1'$).

To asymptotically evaluate $\vec{J}_1^{f'}$, (13) is introduced in (14) and the order of integration is changed. Assuming small losses in the surrounding medium allows the integral on z_1' to be expressed in a closed-form, thus leading to the spectral representation

$$\vec{J}_1^{f'} = \frac{1}{2\pi j} \int_{C_{\theta_1}} \vec{J}_{1\infty}^d(\theta_1) \frac{\sin\theta_1}{(\cos\beta_1' - \cos\theta_1)} d\theta_1. \qquad (15)$$

The integrand in (15) exhibits a pole at $\theta_1 = \beta_1'$; owing to the vanishing losses we have assumed, a counterclockwise indentation of the integration path around this pole is required.

The phase term $\exp(-jkr\cos(\theta_1 - \beta_1))$, which appears in the expression of $\vec{J}_{1\infty}^d(\theta_1)$ provides a saddle point at $\theta_1 = \beta_1$. The contour C_{θ_1} is now deformed onto the steepest descent path (SDP) through this saddle point; in this deformation, the pole at $\theta_1 = \beta_1'$ whose residue represents the singly diffracted field $\vec{J}_1^d$ is captured when $\beta_1 < \beta_1'$. To evaluate the integral on the SDP, the modified Pauli–Clemmow method is then applied as in the UTD [2], thus, leading to the vertex contribution $\vec{J}_1^v$. Finally, the representation (3) is obtained, in which

$$\vec{J}_1^d = U(\beta_1' - \beta_1) \vec{J}_{1\infty}^d(\beta_1') \qquad (16)$$

and

$$\vec{J}_1^v = \vec{J}_1^{vH} + \vec{J}_1^{vE} \qquad (17)$$

where

$$\vec{J}_1^{vH} = -2H_{\beta_1'}^i \frac{F(kr\eta_1)}{(\cos\beta_1' - \cos\beta_1)} \frac{1}{\cos\left(\dfrac{\phi_1'}{2}\right)}$$
$$\times \left[\frac{e^{-jkr}}{2\pi jkr} F(kr\delta_1)\hat{r} - \frac{F_s(kr\delta_1)\cos\beta_1}{4\pi(kr)^2 \sin^2\beta_1} e^{-jkr}\hat{z}_1 \right] \qquad (18)$$

$$\vec{J}_1^{vE} = -2H_{\phi_1'}^i \frac{e^{-jkr}}{4\pi(kr\sin\beta_1)^2} \frac{\sin\left(\dfrac{\phi_1'}{2}\right) F_s(kr\delta_1)}{\cos^2\left(\dfrac{\phi_1'}{2}\right)}$$
$$\times \frac{F(kr\eta_1)}{(\cos\beta_1' - \cos\beta_1)} \hat{z}_1. \qquad (19)$$

In (18) and (19)

$$\eta_1 = 2\sin^2\left(\frac{\beta_1' - \beta_1}{2}\right) \qquad (20)$$

and

$$\delta_1 = 2\sin^2\beta_1 \cos^2\left(\frac{\phi_1'}{2}\right). \qquad (21)$$

The contributions $\vec{J}_1^{dH}$ in (16) is exactly the same as that for the infinite half plane except for a unit-step function U that drops these contributions to zero when passing the SBL $\beta_1 = \beta_1'$. This guarantees a good approximation of the currents very close to the edge and sufficiently far from the vertex; indeed, the representation of the half-plane current in (5)–(7) is exact.

The representation in (3) is continuous everywhere. Indeed, the discontinuity of $\vec{J}_1^{dH}$ and $\vec{J}_1^{dE}$ at the SBL is compensated by $\vec{J}_1^{vE}$ and $\vec{J}_1^{vH}$, that exhibit there the appropriate opposite discontinuity, i.e.,

$$\lim_{\beta_1 - \beta_1' \to 0^{\mp}} \vec{J}_1^{vH, E} = \mp\frac{1}{2} \vec{J}_1^{dH, E}. \qquad (22)$$

The above expression is deduced by the approximation $F(x) \simeq \sqrt{\pi jx}$ of the UTD transition function for a small value of its argument.

It is now useful to discuss the asymptotic behavior of the various contributions. Far out from the SBL's, $\vec{J}_1^{dH}$ and $\vec{J}_1^{dE}$ decay as $(kr)^{-1/2}$ and $(kr)^{-3/2}$, respectively. The contribution $\vec{J}_1^{dE}$ is asymptotically weaker because the soft BC's force to zero the $(kr)^{-1/2}$ terms of the diffracted field.

When the incident plane wave crosses the grazing direction ($\phi_1' = \pi$), an abrupt swap between the lit and the shadowed face occurs so that the PO current (H-case) or its derivative (E-case) exhibits a discontinuity due to the inversion of the normal to the lit face. Consequently, close to $\phi_1' = \pi$, $\vec{J}_1^{dH}$, and $\vec{J}_1^{dE}$ change their spreading factor into $(kr)^0$ and $(kr)^{-1/2}$, respectively, to compensate for this discontinuity.

The dominant contribution of the vertex current $\vec{J}_1^{vH}$ asymptotically decay as $(kr)^{-1}$, owing to the spherical spreading of the scattered power density. It is directed along $\hat{r}$, since the magnetic field of each vertex ray is transverse to the same ray. Close to the SBL ($\beta_1 = \beta_1'$), $\vec{J}_1^{vH}$ becomes of the same order $(kr)^{-1/2}$ of $\vec{J}_1^{dH}$ to compensate for its disappearance. Analogously, $\vec{J}_1^{vE}$ is of order $(kr)^{-1/2}$ and grows up to the order $(kr)^{-3/2}$ close to the SBL. In the following section, the current induced by the DD rays and its relevant vertex contribution are derived.

IV. Current Induced by Doubly Diffracted Rays and by Vertex Rays of the Second Kind

The first step in deriving the DD contribution consists on properly defining and interpreting the diffracted wave from edge 1 that illuminates edge 2. To this end, the magnetic diffracted field is decomposed into the two contributions H_{t_1} and H_{s_1} along $\hat{t}_1$ and $\hat{s}_1$, respectively, where $\hat{s}_1$ is the direction of the singly diffracted grazing ray and $\hat{t}_1$ is the unit vector transverse to the grazing ray. Only the field relevant to the $\vec{J}_1^d$ will be considered, while that associated with $\vec{J}_1^v$ will be neglected because of its higher order. At each point z_2' of the second edge, the contribution H_{t_1} is defined as

$$H_{t_1}(z_2') = (\vec{J}_1^d \times \hat{n}) \cdot \hat{t}_1 \tag{23}$$

where $\hat{n}$ normal to the top face. The contribution H_{s_1} can be expressed in terms of the electric field component E_{t_1}

$$H_{s_1} = -\frac{\partial}{jk\zeta\partial n}(E_{t_1}) \tag{24}$$

so that it can be interpreted as the normal derivative of an E-polarized grazing plane wave. Owing to this E-polarization, the latter wave produces a slope-type DD field contribution, which is of order $(kr)^{-2}$ when observed out from the face and of order $(kr)^{-3}$ just on the face. Consequently, H_{s_1} produces a DD current contribution that can be neglected in our asymptotic expansion.

The magnetic field $H_{t_1}(z_2')$ can be interpreted as a local H-polarized plane wave. This wave excites, at any point z_2', an incremental current contribution $\vec{i}_2^d(z_2')$ that according to the ITD localization process is defined as

$$\vec{i}_2^{dH}(z_2') = \frac{k}{2\pi}\int_{C_{\theta_2}} \vec{j}_{2\infty}^{dH}(\theta_2)\sin\theta_2 e^{jkz_2'\cos\theta_2}\,d\theta_2 \tag{25}$$

in which $\vec{J}_{2\infty}^{dH}(\theta_2)$ is derivable from $\vec{J}_{1\infty}^{dH}(\beta_1')$ in (6), by accomplishing the following operations: 1) substituting 1 with 2 and changing sign; 2) normalizing with respect to the incident field; 3) setting $\phi_2' = 0$; and 4) changing β_2' with θ_2. This leads to

$$\vec{J}_{2\infty}^{dH}(\theta_2) = \vec{j}(\theta_2)e^{-jkr\cos(\beta_2-\theta_2)} \tag{26}$$

in which

$$\vec{j}(\theta_2) = \frac{2}{(2\pi jkr\sin\beta_2\sin\theta_2)^{1/2}}$$
$$\times\left[F(2kr\sin\beta_2\sin\theta_2)\hat{s}_2(\theta_2) \right.$$
$$\left. + \frac{F_s(kr\sin\beta_2\sin\theta_2)\cos\theta_2}{2jkr\sin\beta_2\sin\theta_2}\hat{z}_2 \right]. \tag{27}$$

As depicted in Fig. 4(b), the contribution $\vec{J}_1^{f''}$ is obtained by weighting each incremental current contribution $\vec{i}_2^{dH}$ by the pertinent incident field in (23) and by integrating along the semi-infinite extent of the second edge, i.e.,

$$\vec{J}_1^{f''} = \int_0^\infty H_{t_1}(z_2')\vec{i}_2^{dH}(z_2')\,dz_2. \tag{28}$$

The asymptotic evaluation of this integral provides two contributions. The first one is associated to the stationary phase point that occurs at Q_2'' (Fig. 2) and provides $\vec{J}_1^{dd}$; the second contribution $\vec{J}_1^{vv}$ arises from the end-point at the vertex and provides the desired continuity of the currents $\vec{J}_1^{f''}$ at the SBL ($\beta_2 - \beta_1' - \Omega$) of the DD rays, namely, when both the points Q_1'' and Q_2'' disappear from the vertex. The integral in (28) is asymptotically evaluated in the Appendix, thus leading to

$$\vec{J}_1^{f''} = \vec{J}_1^{ddH} + \vec{J}_1^{vvH} + \vec{J}_1^{vvE} \tag{29}$$

as shown in (30)–(37), at the bottom of the next page. In (31) the upper (lower) sign applies to $\phi_1' < \pi$ ($\phi_1' > \pi$). The transition function

$$W(x) = e^{x^2/4}\sqrt{x}D_{-(1/2)}(x) \tag{38}$$

is the same as that is used in [21] in which

$$D_{-(1/2)}(x) = e^{j(\pi/4)}\frac{e^{x^2/4}}{\sqrt{2\pi}}\int_{-\infty}^{\infty+j0^+}\frac{e^{-((t^2/2)-jxt)}}{\sqrt{t}}\,dt \tag{39}$$

is a cylinder parabolic function of order $-\frac{1}{2}$; in [21], an efficient algorithm is suggested for its numerical calculation. It is worth while to stress that the DD term $\vec{J}_1^{ddE}$ is of order $(kr)^{-3}$ and has been neglected in the above formulation.

The function $W(x)$ is defined in such a way to become one for a large argument that is far from the SBL of the DD rays ($\beta_2 = \beta_1' - \Omega$), thus allowing $\vec{J}_1^{Hdd}$ to recover exactly the DD grazing ray as predicted by UTD. In particular, far from this SBL and when the incident field is far from the grazing aspect, both the contributions $\vec{J}_1^{ddH}$ and $\vec{J}_1^{vvH}$ are of order $(kr)^{-1}$. When the incident plane wave approach $\phi_1' = \pi$, they become of order $(kr)^{-1/2}$ to compensate for the discontinuity of the singly diffracted rays.

In the transition region close to the SBL of the DD rays, the two DD points merge and both the argument of W in (30) and (31) tend to vanish; thus, W also vanishes. At the same time, a square-root-type singularity within $\vec{J}_1^{Hvv}$ and $\vec{J}_1^{Hdd}$ occurs so that the transition function W provides during the transition a uniform of the sum of these. This continuity can be proved in the same way as that demonstrated in [21, Appendix B]. Inside this DD rays transition region, both the terms $\vec{J}_1^{ddH}$ and $\vec{J}_1^{vvH}$ elsewhere of the order $(kr)^{-1}$ become

of order $(kr)^{-3/4}$. It is also worth noting that the transition region provided by $W(x)$ is very narrow when compared with the transition region of the familiar UTD transition function $F(x)$.

V. NUMERICAL RESULTS

The results from the present formulation are compared with those the exact solution [7], which are reported in [12]. Figs. 5–7 are relevant to a plane angular sector with $\Omega = 90°$, which is illuminated as depicted in the insets. These figures show the amplitude of the total radial currents $J_r = (\vec{J}^{PO} + \vec{J}_1^f + \vec{J}_2^f) \cdot \hat{r}$ against the angle β_1, at a distance r from the tip. Our solution (continuous line) is compared with the exact solution (dashed line, from [12]) and with the first-order solution without vertex contribution ($[\vec{J}^{PO} + \vec{J}_1^d + \vec{J}_2^d] \cdot \hat{r}$, dotted line). This latter is the same as the one obtained by applying UTD, except for the fact that the reactive components along $\hat{z}_n$ [see (6) and (7)] have also been included.

For the case in Fig. 5 ($r = 0.5\lambda$), the illumination is such that DD contributions do not occur. The first-order solution without vertex contribution exhibits discontinuities at the two SBL's ($\beta_1 \simeq 38°$ and $\beta_1 \simeq 52°$) that are uniformly compensated by the first-order vertex contributions; the total calculated current well agree with that of the exact solution.

In both the case of Fig. 6(a) ($r = 1.2\lambda$) and 6(b) ($r = 0.5\lambda$), the vertex contribution $\vec{J}^v$ provides the expected continuity
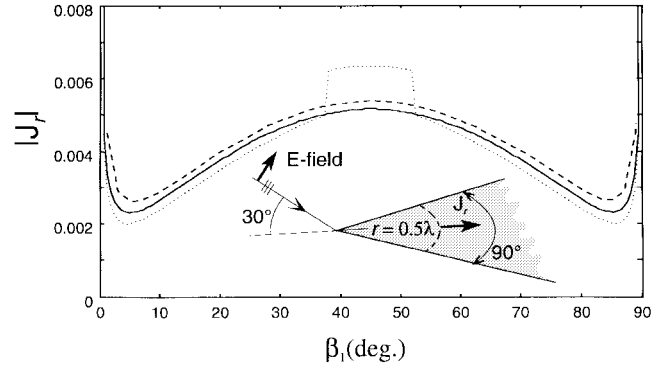

Fig. 5. Amplitude of the radial currents J_r versus β_1 on a plane angular sector with $\Omega = 90°$ at a distance $r = 0.5\lambda$ from the tip. The plane of incidence contains the bisectrix of the angular sector and the incidence aspect is at 150° from the face; the polarization is parallel to the incidence plane. Exact solution (dashed line) - - - -; singly diffracted ray solution (dotted line) $\cdots$; ITD solution (continuous line) ———.

to the total current at the SBL of the singly diffracted rays ($\beta_1 \simeq 38°$). The SBL of the DD rays occurs at $\beta_1 \simeq 52°$ in both Fig. 6(a) and (b); at these aspects, the discontinuity of the DD current $\vec{J}^{dd}$ is smoothly compensated by the relevant $\vec{J}^{vv}$ term. The contribution $\vec{J}^{dd} + \vec{J}^{vv}$ provides, in both cases, a good agreement with the exact solution.

In Fig. 7 the radial current is plotted versus the distance from the tip, at 1° from an edge. Our solution exhibits a

$$\vec{J}_1^{Hdd} = -2H_{\beta_1'}^i \frac{e^{-jkr \cos(\beta_1' - \Omega - \beta_2)}}{2\pi jkr} \frac{F(kr\mu_1^{dd})W(\sqrt{kr}\sigma_1)U(\beta_1' - \Omega - \beta_2)}{\cos\left(\frac{\phi_1'}{2}\right)\sqrt{\sin(\beta_1' - \Omega - \beta_2)\sin\beta_1'\sin\beta_2\sin\Omega}}$$

$$\times \left[F(kr\nu_1^{dd})[\sin(\beta_1' - \Omega - \beta_2)\hat{\beta}_2 + \cos(\beta_1' - \Omega - \beta_2)\hat{r}] + \frac{F_s(kr\nu_1^{dd})\cos(\beta_1' - \Omega)}{2jkr\sin\beta_2\sin(\beta_1' - \Omega)}\hat{z}_2 \right] \quad (30)$$

and

$$\vec{J}_1^{Hvv} = -2H_{\beta_1'}^i \frac{e^{-jkr}}{2\pi jkr} \frac{F(kr\mu_1^{vv})U(\beta_1' - \Omega)}{\left(\left| \cos\frac{\phi_1'}{2} \right| \sqrt{2\sin\beta_1'\sin\Omega} + \sqrt{\cos(\beta_1' - \Omega) - \cos\beta_2} \right)}$$

$$\times \left[\frac{\pm W(j\sqrt{kr}\sigma_1)}{\sqrt{\cos(\beta_1' - \Omega) - \cos\beta_2}} + \frac{\cos\left(\frac{\phi_1'}{2}\right)\cos^2\beta_1'}{\sqrt{2\sin\beta_1'\sin\Omega}} \right] \left[F(kr\nu_1^{vv})\hat{r} + \frac{F_s(kr\nu_1^{vv})\cos\beta_2}{2jkr\sin^2\beta_2}\hat{z}_2 \right] \quad (31)$$

$$\vec{J}_1^{Evv} = 2H_{\phi_1'}^i \frac{e^{-jkr}}{2\pi jkr} \frac{F(kr\mu_1^{vv})\sin\left(\frac{\phi_1'}{2}\right)\cos\beta_1'}{\left| \cos\left(\frac{\phi_1'}{2}\right) \right| \sqrt{2\sin\Omega\sin\beta_1'} + \sqrt{\cos(\beta_1' - \Omega) - \cos\theta_2}} \frac{U(\beta_1' - \Omega)}{\sqrt{2\sin\beta_1'\sin\Omega}}$$

$$\times \left[F(kr\nu_1^{vv})\hat{r} + \frac{F_s(kr\nu_1^{vv})\cos\beta_2}{2jkr\sin^2\beta_2}\hat{z}_2 \right] \quad (32)$$

$$\mu_1^{dd} = \cos(\beta_1' - \Omega - \beta_2) - \cos(\beta_2 - \beta_2') \quad (33)$$

$$\nu_1^{dd} = 2\sin(\beta_1' - \Omega)\sin\beta_2 \quad (34)$$

$$\mu_1^{vv} = 2\sin^2\left(\frac{\beta_1' - \Omega - \beta_2'}{2}\right) \quad (35)$$

$$\nu_1^{vv} = 2\sin^2\beta_2 \quad (36)$$

$$\sigma_1 = 2e^{-j(\pi/4)}\left|\sin\tfrac{1}{2}(\beta_1' - \Omega - \beta_2)\right|. \quad (37)$$
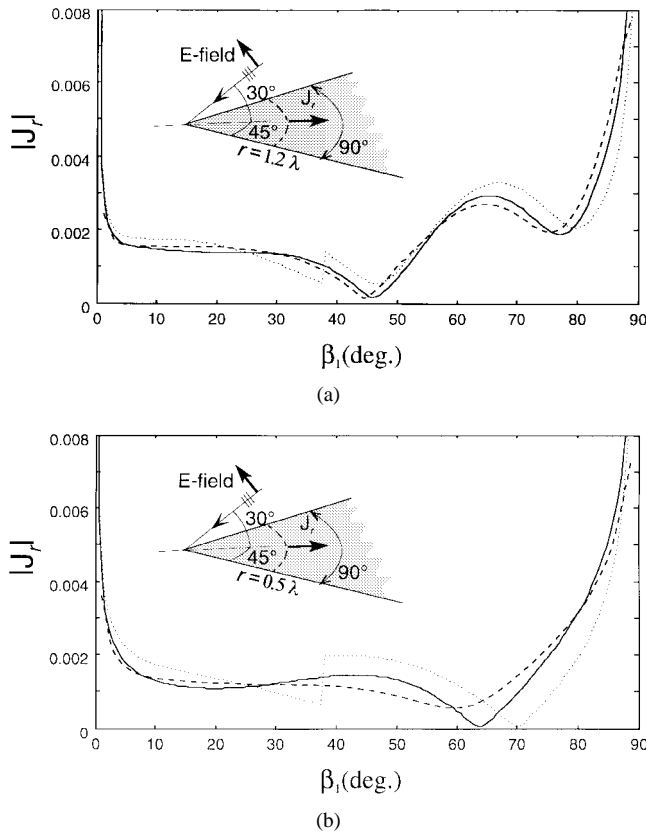
(a)

(b)

Fig. 6. Amplitude of the radial currents versus β_1 at a distance (a) $r = 0.5\lambda$ and (b) $r = 1.2\lambda$ from the tip. The incidence aspect is at $30°$ from the face. Exact solution (dashed line) - - - -; singly diffracted ray solution (dotted line) $\cdots$; and ITD solution (continuous line) ———.
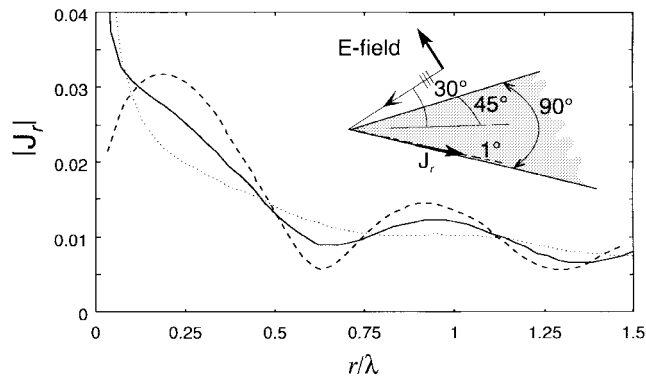

Fig. 7. Amplitude of the radial currents versus r at $\beta_1 = 1°$ from edge 1. The incidence aspect is at $30°$ from the face. Exact solution (dashed line) - - - -; singly diffracted ray solution (dotted line) $\cdots$; and ITD solution (continuous line) ———.

reasonable agreement with the exact solution. This latter shows a more oscillatory behavior that induces one to think that an additional contribution arising from the vertex occurs; due to the vicinity to the edge, this can be attributed to edge waves [27], that have been neglected in the present solution.

Fig. 8 shows an example in which the double diffraction contribution and the vertex contributions play an important role; a plane angular sector with $\Omega = 60°$ is illuminated from a direction $\beta_1' = 100°$, $\phi_1' = 160°$ with an E-field along $(\frac{1}{2}\hat{\beta}_1' + (\sqrt{3}/2)\hat{\phi}_1')$. The total current (continuous line) are
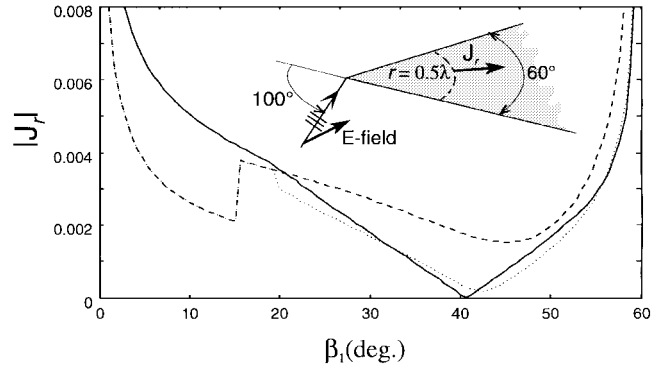

Fig. 8. Amplitude of the radial currents J_r versus β_1 at $r = 0.5\lambda$ on a plane angular sector with $\Omega = 60°$; the incidence aspect has $\beta_1' = 100°$ and $\phi_1' = 160°$. The polarization is along $\frac{1}{2}B_i + (\sqrt{3}/2)\hat{\phi}_1'$. Total current (continuous line) ———; $\vec{J}^d \cdot \hat{r}$ (dashed line) - - - -; and $(\vec{J}^{dd} + \vec{J}^d) \cdot \hat{r}$ (dotted line) $\cdots$.

compared with $\vec{J}^d \cdot \hat{r}$ (dashed line) and with $(\vec{J}^{dd} + \vec{J}^d) \cdot \hat{r}$ (dotted line). It is found that $\vec{J}^{dd}$ provides a significant contribution where it exists ($\beta_1 > 20°$) due to the fact that the plane wave is close to grazing. By comparing the curves, it can also be deduced that the term $\vec{J}^v$ is important from β_1 ranging from 0 to $18°$ and that $\vec{J}^{vv}$ compensates well for the discontinuities of $\vec{J}^{dd}$ at $\beta_1 = 20°$.

In the results presented next, the currents of the present formulation are used in a radiation integral for calculating the far-field pattern of flat polygonal plates. In particular, the fringe currents of each corner of the plate are integrated over the finite-plate surface, obviously retaining only one time the fringe contribution due to the singly diffracted rays arising from the same edge. The test cases that have been chosen are the same as that in [18], so that our results can be compared with other approaches based on first- and second-order PTD [18]. It is worth noting that the integration of our fringe currents over the finite surface of the plate introduce an end-point-type description of the diffraction contributions associated to the following additional mechanisms:

1) interaction between nonadjacent edges;
2) interaction of each vertex with nonadjacent edges;
3) interaction between the DD field of two adjacent edge with a third edge (triple diffraction).

The above interactions are described here only by abruptly truncating the integration domain without introducing the correct half-plane diffracted field at the nonadjacent edge. Furthermore, corner-to-corner and edge-wave effects are not correctly described.

In Fig. 9, the bistatic RCS of the square plate depicted in the inset is presented; the two contributions $\sigma_{\phi\theta'}$ and $\sigma_{\theta\phi'}$ are shown in Fig. 9(a) and 9(b), respectively. The numerical results from the present formulation (continuous line) are compared with those from an MoM solution (dashed line, from [18]) The agreement is quite satisfactory. In the same figure, calculations are presented (dotted line) that have been calculated by applying the diffraction coefficients obtained in [20], which are the nonuniform (far-field) version of those derived in [21]. The two high-frequency methods very closely compare, as expected, except for aspects close to grazing, were
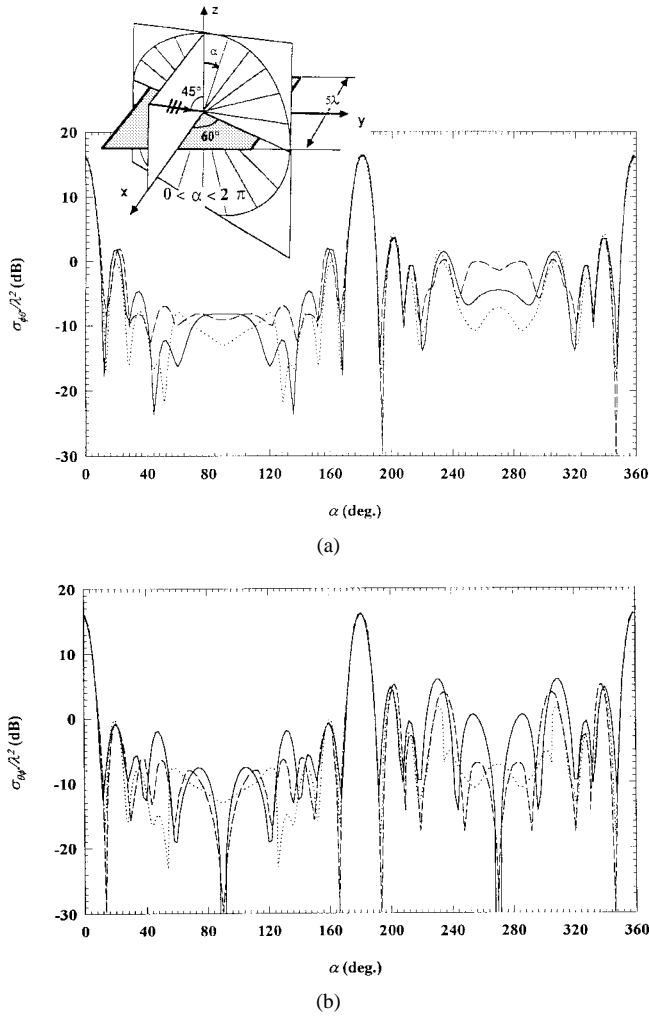
Fig. 9. Bistatic echo area of a 5λ square plate. (a) $\sigma_{\phi\theta}$. (b) $\sigma_{\theta\theta}$, ($\phi' = 0$; $\theta' = 45°$); ———— integration of ITD currents; - - - - MoM (from [18]); $\cdots\cdots$ solution presented in [20]).

Fig. 10. Monostatic echo area of a triangular plate. (a) $\sigma_{\theta\theta'}$. (b) $\sigma_{\phi\phi'}$; ———— integration of ITD currents; - - - - MoM (from [17]); ———— solution presented in [18].

the present solution provides better agreement with MoM. This may be attributed to the additional end-point-type descriptions of the interaction mechanisms 1)–3) that are not included by our previous solution [20]. This is particularly evident in Fig. 9(b), where the present solution, unlike [20], predicts vanishing field at grazing aspects, as expected from physical considerations.

Finally, Fig. 10 shows the monostatic copolar RCS on the principal plane of a 30° isosceles triangular plate. As pointed out in [18], this case is particularly difficult to simulate in high-frequency regime, since vertex diffraction from a very acute angle and vertex/edge interactions via edge waves play an important role at grazing aspects. In particular, for the case of polarization parallel to the plate [Fig. 10(a)], our prediction fails close to nose-on incidence due to the presence of significant edge-wave effects. Including these effects produces improvement, as appears in the solution from [18] (also reported here for convenience). For polarization at grazing incidence, which is orthogonal to the plate [Fig. 10(b)], a large lobe at 150° appears that is not completely reconstructed neither by our solution nor by the inclusion of the edge-wave contributions. In [12], it is demonstrated that a more
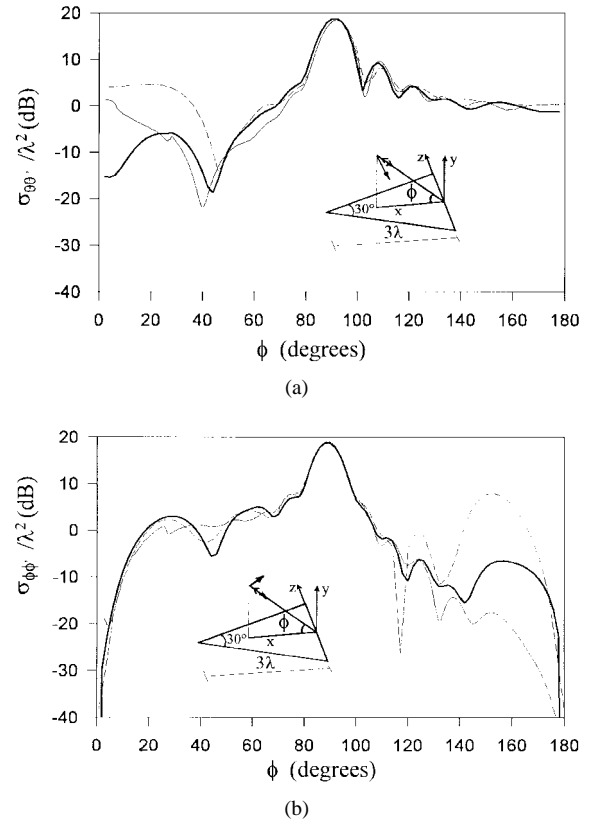
adequate prediction for this case is obtained by using a vertex current correction directly derived from the exact solution [7]. This stresses again that the vertex contribution of the present solution should be improved for narrow corner angle.

VI. CONCLUSIONS

High-frequency expressions of the currents induced by the diffracted field on a plane angular sector have been derived on the basis of the ITD. Both singly and DD fringe currents have been accounted for and two types of vertex fringe currents are also introduced; these latter contributions provide the continuity of the currents induced by both singly and DD rays, respectively. The final expressions have been obtained in terms of the familiar UTD transition function, and of a cylinder parabolic transition function which is very simple to compute [21].

In deriving the present high-frequency solution, the reactive components of the half-plane canonical field are retained into the ITD solution, so that the final expressions tend to reconstruct the near-edge behavior at a certain distance from the tip. The currents close to the vertex are not correctly estimated by the present formulation, especially for narrow corner angles. However, it is found that it provides satisfactory results for a 90° corner also at a half wavelength from the tip.

A part from the prediction of the scattered field from polygonal plates in both far and near zone, a further application of this formulation regards the description of the radiation pattern of aperture antennas on finite ground planes. Indeed,

by using reciprocity, the tangent magnetic field on a plane angular sector (which is directly related to the current of our formulation) can be interpreted as the normalized far-field radiated by an elementary magnetic dipole located on the same angular sector.

APPENDIX

In order to asymptotically evaluate the integral (28) for kr large, (25) is introduced in (28); after changing the order of integration this leads to

$$\vec{J}_1^{f''} = U(\beta_1' - \Omega)\left(-H_{\beta_1'}^i\left(2\vec{\mathfrak{T}}_1 + 4\vec{\mathfrak{T}}_2 \cos^2\left(\frac{\phi_1'}{2}\right)\cos^2\beta_1'\right) + 4H_{\phi_1'}^i \vec{\mathfrak{T}}_2 \sin\frac{\phi_1'}{2} \cos\frac{\phi_1'}{2} \cos\beta_1'\right) \tag{40}$$

where

$$\vec{\mathfrak{T}}_i = \frac{k}{2\pi}\int_{C_{\theta_2}} \vec{j}(\theta_2)A_i(\theta_2)e^{-jkr\cos(\beta_2-\theta_2)}\sin\theta_2\, d\theta_2, \quad i = 1, 2 \tag{41}$$

and

$$A_i(\theta_2) = \int_0^\infty \frac{\frac{1}{2}[1-(-1)^i]-(-1)^i F(\gamma_1 z_2)}{\pm\sqrt{j\pi\gamma_1 z_2}} \times e^{-jk[\cos(\beta_1'-\Omega)-\cos\theta_2]z_2}\, dz_2 \tag{42}$$

in which $F(x)$ is the UTD transition function defined in (10) and

$$\gamma_1 = 2k\sin\Omega\sin\beta_1'\cos^2\left(\frac{\phi_1'}{2}\right). \tag{43}$$

The integrals in (42) can be calculated in the exact closed-form [28, eq. 6.283]

$$A_1(\theta_2) = \frac{a(\theta_2)}{\sqrt{\cos(\beta_1'-\Omega)-\cos\theta_2}} \tag{44}$$

$$A_2(\theta_2) = \frac{a(\theta_2)}{\left|\cos\left(\frac{\phi_1'}{2}\right)\right|\sqrt{2\sin\beta_1'\sin\Omega}}. \tag{45}$$

The term $a(\theta_2)$, shown in (46) at the bottom of the page, exhibits a branch point singularity at $\theta_2 = \beta_1' - \Omega$; the branch cut is chosen in such a way that $\mathrm{Im}[\sqrt{\cos\theta_2 - \cos(\beta_1'-\Omega)}] > 0$ in the top Rieman sheet of the complex θ_2 plane. The two integrals $\vec{\mathfrak{T}}_1$ and $\vec{\mathfrak{T}}_2$ obtained using (44) and (45) inside (41) are of the same type as that obtained in [21, eq. (35)], and can be calculated with the same technique; this leads to

$$\vec{\mathfrak{T}}_1 = \vec{\mathfrak{T}}_1^{dd} + \vec{\mathfrak{T}}_1^{vv} \tag{47}$$

$$\vec{\mathfrak{T}}_1^{vv} \sim (\vec{\mathfrak{T}}_1^{vv})_{nu} W\left(j\sqrt{kr}\sigma_1\right)F(kr\mu_1^{vv}) \tag{48}$$

$$\vec{\mathfrak{T}}_1^{dd} \sim (\vec{\mathfrak{T}}_1^{dd})_{nu} W\left(\sqrt{kr}\sigma_1\right)F(kr\mu_1^{dd})U(\beta_1'-\Omega-\beta_2) \tag{49}$$

where $(\vec{\mathfrak{T}}_1^{dd})_{nu}$ and $(\vec{\mathfrak{T}}_1^{vv})_{nu}$ derive from nonuniform approximation of the stationary phase-point contribution and of the end-point contribution, respectively, of the integral in (41)

$$(\vec{\mathfrak{T}}_1^{dd})_{nu} = \frac{e^{-jkr\cos(\beta_1'-\Omega+\beta_2)}}{\sqrt{kr}}\frac{k\sqrt{j}}{2\sqrt{2\pi}} \times \frac{\vec{j}(\beta_1'-\Omega)a(\beta_1'-\Omega)\sin(\beta_1'-\Omega)}{\sqrt{\sin(\beta_1'-\Omega)\sin(\beta_1'-\Omega-\beta_2)}} \tag{50}$$

$$(\vec{\mathfrak{T}}_1^{vv})_{nu} = \frac{e^{-jkr}}{\sqrt{kr}}\frac{k\sqrt{j}}{\sqrt{2\pi}}\vec{j}(\beta_2)A_1(\beta_2)\sin\beta_2. \tag{51}$$

From (47)–(51), it is a straightforward matter to obtain (30)–(32).

The technique for deriving (48) and (49) is discussed in [21] and is summarized here. As a first step, the incidence aspect is supposed to be far from grazing (ϕ_1' far from π) and an asymptotic evaluation is accomplished, which is uniformly valid across the SBL of the DD rays ($\beta_2 = \beta_1' - \Omega$). For obtaining this, the contour is deformed into a SDP through the point $\theta_2 = \beta_2$ on the top Rieman sheet. The integration along the SDP gives the $\vec{J}_1^{vv}$ contribution. In this deformation, the branch point singularity at $\beta_1' - \Omega$ is captured when $\beta_2 < \beta_1' - \Omega$ so that an integration along a contour around the branch cut has to be included, which is asymptotically dominated by the branch point. This latter integration leads to the contribution $\vec{J}_1^{dd}$. The uniform description of the field at the SBL (merging between saddle point and branch point) is treated by introducing the transition function W. As a second step, the observation point is supposed to be far from the above SBL, and an asymptotic evaluation is carried out which is also valid for near-grazing incidence. Finally, uniform expressions of the currents are deduced from the previous steps, which are valid everywhere except when simultaneously $\phi_1' = \pi$ and $\beta_2 = \beta_1' - \Omega$ that corresponds to the special case in which the SBL's of singly and DD rays merge. However, also in this pathological situation, our solution remains well-behaved and numerically stable.

ACKNOWLEDGMENT

REFERENCES

[1] J. B. Keller, "Geometrical theory of diffraction," *J. Opt. Soc. Amer.,* vol. 52, pp. 116–130, 1962.
[2] R. G. Kouyoumjian and P. H. Pathak, "A uniform geometrical theory of diffraction for an edge in a perfectly conducting surface," *Proc. IEEE,* vol. 62, pp. 1448–1461, Nov. 1974.
[3] P. Y. Ufimtsev, "Method of edge waves in the physical theory of diffraction," transl. by U.S. Air Force Foreign Technol. Div., Wright-Patterson AFB, OH, 1971.

$$a(\theta_2) = \frac{\pm 1/jk}{\left/\cos\left(\frac{\phi_1'}{2}\right)\right/\sqrt{2\sin\Omega\sin\beta_1'} + \sqrt{\cos(\beta_1'-\Omega)-\cos\theta_2}} \tag{46}$$

[4] _____, "Elementary edge waves and the physical theory of diffraction," *Electromagn.,* vol. 11, no. 2, pp. 125–159, Apr.–June 1991.

[5] J. Radlow, "Note on the diffraction at a corner," *Arch. Rational. Mech., Anal.,* vol. 19, pp. 62–70.

[6] N. C. Albertsen, "Diffraction by a quarterplane from a half-wave dipole," *Proc. Inst. Elect. Eng.,* vol. 144, pt. H, no. 3, pp. 191–196, June 1997.

[7] R. S. Satterwhite and R. G. Kouyoumjian, "Electromagnetic diffraction by a perfectly conducting plane angular sector," Tech. Rep. 2183-2, ElectroScience Laboratory, The Ohio State Univ., under Contract AF19(628)-5929 for Air Force Cambridge Res. Labs., Bedford, MA, 1970.

[8] R. S. Satterwhite, "Diffraction by a quarter plane, the exact solution and some numerical results," *IEEE Trans. Antennas Propagat.,* vol. AP-22, no. 3, pp. 500–503, Mar. 1974.

[9] T. B. Hansen, "Diffraction by a plane angular sector, a new derivation," *IEEE Trans. Antennas Propagat.,* vol. AP-38, pp. 1892–1894, Nov. 1990.

[10] V. P. Smyshlyaev, "Diffraction by conical surfaces at high-frequency," *Wave Motion,* vol. 12, pp. 329–339, 1990.

[11] _____, "The high-frequency diffraction of electromagnetic waves by cones of arbitrary cross-section," *Soc. Indust. Appl. Math.,* vol. 53, no. 3, pp. 670–688, 1993.

[12] T. J. Brinkley and R. J. Marhefka, "Current near the vertex of perfectly conducting angular sector," *IEEE Trans. Antennas Propagat.,* to be published.

[13] T. B. Hansen, "Corner diffraction coefficients for the quarter plane," *IEEE Trans. Antennas Propagat.,* vol. 39, pp. 976–984, July 1991.

[14] K. H. Hill, "A UTD solution to the EM scattering by the vertex of a perfectly conducting plane angular sector," Ph.D. dissertation, Dept. Elect. Eng., The Ohio State Univ., Columbus, OH, 1990.

[15] L. P. Ivrissimtzis and R. J. Marhefka, "Double diffraction at a coplanar skewed edge configuration," *Radio Sci.,* vol. 26, pp. 821–830, 1991.

[16] F. Capolino, M. Albani, S. Maci, and R. Tiberio, "Diffraction from a couple of coplanar, skew wedges," *IEEE Trans. Antennas Propagat.,* vol. 45, pp. 1219–1226, Aug. 1997.

[17] M. Albani, F. Capolino, S. Maci, and R. Tiberio, "Diffraction at a thick screen including corrugations on the top face," *IEEE Trans. Antennas Propagat.,* vol. 45, pp. 277–283, Feb. 1997.

[18] L. P. Ivrissimtzis and R. J. Marhefka, "A uniform ray approximation of the scattering by polyhedral structures including higher terms," *IEEE Trans. Antennas Propagat.,* vol. 40, pp. 1302–1312, Nov. 1992.

[19] O. Breinbjerg, "Higher order equivalent edge currents for fringe wave radar scattering by perfectly conducting polygonal plates," *IEEE Trans. Antennas Propagat.,* vol. 40, pp. 1543–1554, Dec. 1992.

[20] S. Maci, R. Tiberio, and A. Toccafondi, "Diffraction at a plane angular sector," *J. Electromagn. Wave Applicat.,* vol. 8, no. 9/10, pp. 1247–1276, Sept. 1994.

[21] F. Capolino and S. Maci, "Uniform high-frequency description of singly, doubly, and vertex diffracted rays for a plane angular sector," *J. Electromagn. Wave Applicat.,* vol. 10, no. 9, pp. 1175–1197, Oct. 1996.

[22] _____, "Simplified, closed-form expressions for computing the generalized Fresnel integral and their application to vertex diffraction," *Microwave Opt. Tech. Lett.,* vol. 9, no. 1, pp. 32–37, May 1995.

[23] R. Tiberio and S. Maci, "Incremental theory of diffraction, scalar formulation," *IEEE Trans. Antennas Propagat.,* vol. 42, pp. 600–612, May 1994.

[24] R. Tiberio, S. Maci, and A. Toccafondi, "Incremental theory of diffraction, electromagnetic formulation," *IEEE Trans. Antennas Propagat.,* vol. 43, pp. 87–96, Jan. 1995.

[25] S. Maci, R. Tiberio, and A. Toccafondi, "Incremental diffraction coefficients for source and observation at finite distance from an edge," *IEEE Trans. Antennas Propagat.,* vol. 44, pp. 593–599, May 1996.

[26] M. Born and E. Wolf, *Principles of Optics Third,* revised ed. Oxford, U.K.: Pergamon, 1965.

[27] L. P. Ivrissimtzis and R. J. Marhefka, "Edge wave vertex and edge diffraction," *Radio Sci.,* vol. 24, no. 6, pp. 771–784, 1989.

[28] I. S. Gradshteyn and I. M. Ryzhik, *Table of Integrals, Series and Products.* San Diego, CA: Academic, 1980, p. 649.

Stefano Maci (M'92), for a photograph and biography, see p. 578 of the April 1998 issue of this TRANSACTIONS.

Matteo Albani (M'97), for a photograph and biography, see p. 578 of the April 1998 issue of this TRANSACTIONS.

Filippo Capolino (M'94), for a photograph and biography, see p. 578 of the April 1998 issue of this TRANSACTIONS.